

Visual-Semantic Graph Attention Network for Human-Object Interaction Detection

Zhijun Liang, Yisheng Guan, and Juan Rojas

Guangdong University of Technology

Abstract

In scene understanding, machines benefit from not only detecting individual scene instances but also from learning their possible interactions. Human-Object Interaction (HOI) Detection tries to infer the predicate on a $\langle \text{subject}, \text{predicate}, \text{object} \rangle$ triplet. Contextual information has been found critical in inferring interactions. However, most works use features from single object instances that have a direct relation with the subject. Few works have studied the disambiguating contribution of subsidiary relations in addition to how attention might leverage them for inference. We contribute a dual-graph attention network that aggregates contextual visual, spatial, and semantic information dynamically for primary subject-object relations as well as subsidiary relations. Graph attention networks dynamically leverage node neighborhood information. Our network uses attention to first leverage visual-spatial and semantic cues from primary and subsidiary relations independently and then combines them before a final readout step. Our network learns to use primary and subsidiary relations to improve inference: encouraging the right interpretations and discouraging incorrect ones. We call our model: Visual-Semantic Graph Attention Networks (VS-GATs). We surpass state-of-the-art HOI detection mAPs in the challenging HICO-DET dataset, including in long-tail cases that are harder to interpret. Code, video, and supplementary information will be made available.

1. Introduction

Human-Object Interaction (HOI) detection has recently gained important traction. The goal is to infer an interaction predicate for the $\langle \text{subject}, \text{predicate}, \text{object} \rangle$ triplet. Whilst computer vision has experienced extraordinary advances in object detection [6, 21, 29], human pose estimation [5, 25], scene segmentation [13], and action recognition [17, 38]; the harder problem of HOI has progressed less so, as it is a more

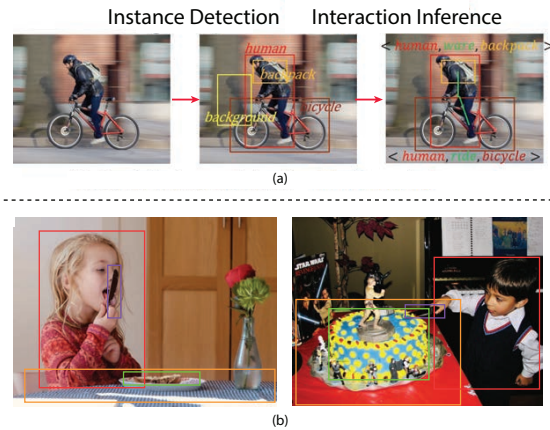


Figure 1. (a) HOI Detection: An object detector extracts subject and object proposals. Proposal features are used by an ‘interaction module’ to infer likely predicates. (b) Primary relation cues infer $\langle \text{human}, \text{hold}, \text{knife} \rangle$ on the left; but on the right $\langle \text{human}, \text{?, cake} \rangle$ the relation is not obvious by simply looking at the human and the cake. Only when the knife and the cake are seen jointly can we disambiguate.

challenging problem. HOI requires better understanding of contextual information for better inference. HOI starts with instance detection (localizing and identifying subject and objects) and continues with interaction inference as illustrated in Fig. 1a.

HOI research typically infers interactions based on the local features of a subject-object pair [3, 8, 9, 21]. Over time, additional contextual cues have been leveraged to improve inference [1, 12, 18, 26, 34, 36]. However, to date, there are still many interactions that confuse our systems. Consider Fig. 1(b) for example. On the left, a girl holds and licks a knife. Primary visual and spatial information can infer so. But what is often not considered is that the subsidiary relations $\langle \text{knife}, \text{table} \rangle$, $\langle \text{human}, \text{table} \rangle$ can help inhibit the system from choosing $\langle \text{cut} \rangle$. On the right, primary relations predict $\langle \text{hold} \rangle$ not $\langle \text{cut} \rangle$. Only when the system

pays attention to the <knife-cake> and <human,cake> subsidiary contextual cues can it infer that <cut> is the right interaction. Researchers have exploited a variety of contextual cues including visual, spatial, semantic, interactiveness, human pose, and functional approximation to better understand a scene. They have also used a variety of architectures including deep neural networks (DNNs), attention, graphs, graph neural nets, and graph attention nets (see Sec. 2 for an overview). However, most works have only leveraged local-primary relations in the scene to infer interactions.

In this paper, we study the disambiguating power of subsidiary scene relations via a double Graph Attention Network that aggregates visual-spatial, and semantic information in parallel. The network uses attention to leverage primary and subsidiary contextual cues to gain additional disambiguating power. Our work is the first to use dual attention graphs. We call our system: Visual-Semantic Graph Attention Networks (VS-GATs).

We begin the HOI task by using instance detection (Sec. 3.2). Then a pair of Graph Attention networks are created. The first graph’s nodes are instantiated from bounding-box visual features; while the edges are instantiated from corresponding spatial features (Sec. 3.3.2). The second graph’s nodes are instantiated from word embedding features associated with corresponding visual nodes (see Sec. 3.3.3). An attention mechanism then updates the node features of each graph and learning from primary and subsidiary contextual relations. A combined graph is created by concatenating both graph’s node features. Then inference is done through a readout step on box-paired subject-object nodes. Fig. 2 offers an overview of our system. Notice the existing edges between subsidiary instances and the human as well as in-between objects. These relations, along with attention mechanism, aid in discerning scenes better. The inference modules is trained and tested in the challenging HICO-DET dataset [3] and surpasses state-of-the-art (SOTA) for the Full and Rare categories with mAPs of 19.66 and 15.79 respectively. The results show the additional attention mechanism from subsidiary contextual cues improves inference even for samples with few training examples. We expect to see improved attention mechanisms learn better contextual cues and continue to improve interaction inference.

2. Related Work

Learning to better understand context is critical to scene understanding. Recently, researchers have exploited visual, spatial, semantic, interactiveness, human pose, and functional approximation as contextual cues. Simultaneously a host of architectures including deep nets, graph nets, and graph attention nets have also been used. In this section we present the works by keying in on the architecture type and then describing the various contexts used therein.

Multi DNN Streams with Various Contextual Cues. A primary way to do HOI has been to extract visual features from instance detectors along with spatial information to instantiate multi-streams of DNNs. Each stream may contain information of detected human(s), objects, and perhaps some representation of interaction. A final fusion step is undertaken where individual inferences scores are multiplied to yield a final one [3,8,9]. Lu *et al.* [22] considered semantic information under the multi-stream DNN setting stating that interaction relationships are also semantically related to each other. Gupta *et al.* [12] and Wan *et al.* [34] emphasized a fine-grained layout of the human pose and leverage relation elimination or interactiveness modules to improve inference. Li *et al.* [17], include an interactiveness network that like Gupta *et al.* eliminates non-interactive edges. Visual, spatial, and pose features are concatenated and input into the interactiveness discriminator which finally outputs a detection classification. Peyre *et al.* [26] and Bansal *et al.* [1] go a step further and consider semantic functional generalization. Bansal *et al.* consider how humans interact with functionally similar objects in similar manners. They leverage word2vec embeddings [23] to train a fixed human-action with other similar object embeddings. Peyre *et al.* [26] use the similar concept of visual analogies. They instantiate another stream using a visual-semantic embedding of the triplet resulting in a triagram. Analogies like functional approximation rely on similarity of function but in this case at a visual level.

Graph Neural Networks. Graph Neural Networks (GNNs) [35] were first conceptualized as recurrent graph neural networks (RecGNNs) [11,30]. RecGNNs learned a target node through neighbor information aggregation until convergence. Afterwards, Convolutional Graph Neural Networks (ConvGNNs) were devised under two main streams: spectral-based [2] and spatial-based approaches [24]. These graphs generalize the convolution operation from a grid to a graph. A node’s representation is created by aggregating self and neighboring features. ConvGNNs stack multiple graph layers to generate high-level node representations. Spatio-temporal Graph Neural Networks simultaneously consider both spatial and temporal dependencies and often leverage ConvGNNs for spatial encoding and RecGNNs for temporal encoding.

GNNs have been used to model scene relations and knowledge structures. Kato *et al.* [16] use an architecture that consists of one stream of convolutional features and another stream composed of a semantic graph. In the latter, verbs and nouns form nodes which use word embeddings as their features. New connected action nodes are inferred. Learning propagates features which are finally merged with visual features from the convolutional network. Note that this work did not classify HOI detections; instead they in-

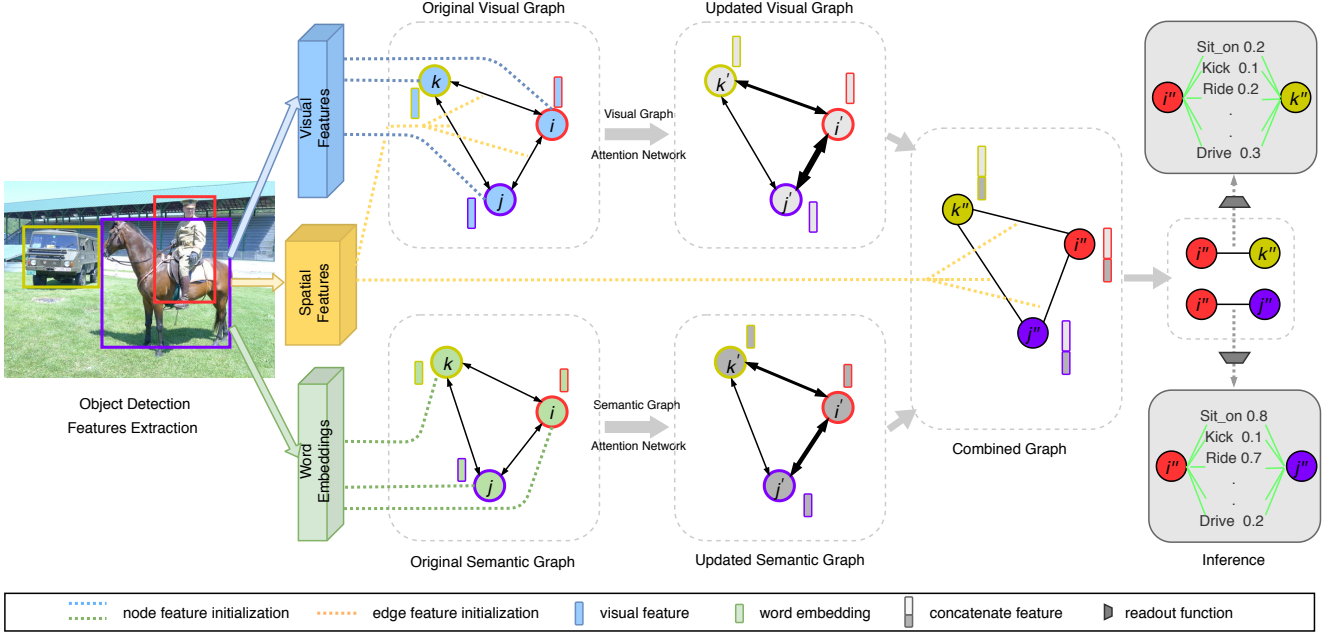


Figure 2. Visual-Semantic Graph Attention Network: After instance detection, a visual-spatial and a semantic graph are created. Node edge weights are dynamically through attention. We combine these graphs and then perform a readout step on box-pairs to infer all possible predicates between one subject and one object.

ferred a single interaction from the global scene. Xu *et al.* [36], similarly use a visual stream with convolutional features for human and object instances and a parallel knowledge graph that yields candidate verb features. The authors lean on the concept of semantic regularities to assert that visual-semantic feature pairs contain semantic structure that needs to be retained. They finish by conducting a multi-modal joint embedding, where the objective maximizes the similarity of positive pairs and minimizes similarity across all non matching pairs.

Graph Attention Networks More recently Velivckovic *et al.* [33] introduced Graph Attention Networks (GATs). GATs operate on graph structured data and leverage masked self-attentional layers. Nodes attend their neighbor’s features and dynamically learn edge-weight proportions with neighbors according to their usefulness.

Yang *et al.* [39] proposed a Graph R-CNN network to learn scene relations visually (not HOI detection). Their system extracts visual features through a region proposal network (RPN) and builds a graph. They learn to prune irrelevant edges and use an attention mechanism to propagate higher-order context throughout the graph. They predict per-node edge attentions and learn to modulate information flow across unreliable or unlikely edges. Sun *et al.* [31], do multi-person action forecasting in video. They use a RecGNN based on visual and spatio-temporal features to create and update the graph. Lastly, Qi *et al.* [28] are the

first to explicitly use a GAT for HOI in images and video. They propose a graph parsing neural net (GPNN) that takes node and edge visual features as input from which a graph is formed. The graph structure is set by an adjacency matrix. Message updates leverage attention mechanisms via a weighted sum of the messages of the other nodes. Finally, a readout function is used for interaction inference.

To date, only Qi *et al.* [28] have used GAT architectures that consider subsidiary relations. We further improve the SOTA by integrating additional contextual cues into the attention mechanism (spatial and semantic ones) through a parallel dual-attention graph architecture and show it’s disambiguating power.

3. Visual-Spatial Graph Attention Network

In this section, we first introduce the notion of a graph, then describe the visual and semantic graphs; their attention mechanisms; the fusion step; inference; training, and finally implementation details.

3.1. Graphs

A graph G is defined as $G = (V, E)$ that consists of a set of V nodes and a set of E edges. Node features and edge features are denoted by \mathbf{h}_v and \mathbf{h}_e respectively. Let $v_i \in V$ be the i th node and $e_{i,j} = (v_i, v_j) \in E$ be the directed edge from v_i to v_j .

A graph with n nodes has a node features matrix $\mathbf{X}_v \in \mathcal{R}^{n \times d}$ and an edge feature matrix $\mathbf{X}_e \in \mathcal{R}^{m \times c}$ where $\mathbf{h}_{v_i} \in$

\mathcal{R}^d is the feature vector of node i and $\mathbf{h}_{e_{i,j}} \in \mathcal{R}^c$ is the feature vector of edge (i, j) . Fully connected edges imply $e_{i,j} \neq e_{j,i}$.

More formally, given an input image I , and interaction class labels \mathbf{R} , then the goal is to infer the joint probability $P(\mathbf{R}, G_C, G_V, G_S | I)$, which can be factorized as:

$$\begin{aligned} P(\mathbf{R}, G_C, G_V, G_S | I) &= P(G_V, G_S | I) \\ &\quad P(G_C | G_V, G_S, I) \\ &\quad P(\mathbf{R} | G_C, G_V, G_S, I). \end{aligned} \quad (1)$$

This factorization serves to design our system. First, $P(G_V, G_S | I)$ is accomplished through the visual-spatial and semantic-GAT graphs of Sec. 3.3.2 and 3.3.3. $P(G_C | G_V, G_S, I)$ is accomplished by combining both graphs as described in Sec. 3.4 and illustrated in Fig. 2. The last factorization $P(\mathbf{R} | G_C, G_V, G_S, I)$ is the inference step accomplished through box-pairing and readout described in Sec. 3.5. Training and implementation detail are also offered in Sec. 3.5.1 and Sec. 3.6 respectively.

3.2. Contextual Features

In this section we describe how contextual features are extracted and later describe how they are used to instantiate nodes and edges in Sec. 3.3.

Visual Features Visual features are extracted from subject and object proposals generated from a two-stage Faster-RCNN (ResNet-50-FPN) [14, 19, 29]. First, the RPN generates (hundreds) of subject and object proposals. Thus, for an image I , the i th human bounding-box b_h^i and the j th object bounding-box b_o^j are used to extract latent features from Faster-RCNNs last fully-connected layer ($FC7$ after the ROI pooling layer) to instantiate the visual graph nodes as described in Sec. 3.3.2.

Note that we use an empirically-derived score threshold to limit the number of subject and object proposals (see Sec. 3.6 for specific numbers). By eliminating non-useful proposals, the system better focuses its resources on the more important relations. Several other works have more sophisticated proposals [12, 18, 39]; we leave this as future work.

Spatial Features Spatial features such as bounding box locations and relative locations are informative about the relationship that proposals have with each other [15, 27, 40, 41]. Spatial features are also useful to encode the predicate. Consider the “ride” predicate, then we can deduce that subject is above the object.

Given a pair of bounding boxes, their paired-coordinates are given by (x_i, y_i, x_2, y_2) and (x'_i, y'_i, x'_2, y'_2) . Along with respective areas A and A' and an image area A^I of size (W, H) .

Spatial features can be grouped into (i) relative scale and (ii) relative position features. Bounding-box relative scale features s_{rs} are defined as:

$$s_{rs} = \left[\frac{x_i}{W}, \frac{y_i}{H}, \frac{x_j}{W}, \frac{y_j}{H}, \frac{A}{A^I} \right]. \quad (2)$$

Relative position bounding-box features s_{rp} are defined as:

$$s_{rp} = \left[\left(\frac{x_i - x'_i}{x_j - x'_i}, \frac{y_i - y'_i}{y_j - y'_i}, \log\left(\frac{x_j - x_i}{x'_j - x'_i}\right), \right. \right. \\ \left. \left. \log\left(\frac{y_j - y_i}{y'_j - y'_i}\right), \frac{x_c - x'_c}{W}, \frac{y_c - y'_c}{H} \right] \right]. \quad (3)$$

The relative position expression is similar to the bounding box regression coefficients proposed in [29], but two center scales are added to yield more obvious cues.

So, the set of spatial features s used in our architecture is the union of these sets $s = s_{rs} \cup s_{rp}$. Spatial features will be used to: (i) build the edges in the Visual graph as described in Sec. 3.3.2 but also as part of the Combined Graph described in Sec. 3.4 in what amounts to a dilated step in neural nets.

Semantic Features In this work, we use word2vec embeddings as semantic features [23]. word2vec takes a text corpus as input and produces latent word vectors \mathbf{w} as outputs. The latent representation retains semantic and syntactic similarity. Similar context is made evident through spatial proximity; indicating that words have mutual dependencies.

We use the publicly available word2vec vectors pre-trained on the Google News dataset (about 100 billion words) [10]. The model yields a 300-dimensional vector for 3 million words and phrases and is trained according to [23]. All existing object classes in the HICO-DET dataset are used to obtain the word2vec latent vector representations offline.

In effect, when instance proposals are suggested by the RPN (Sec. 3.3.2), a set of corresponding class labels are available. word2vec uses these to instantiate the nodes in the semantic graph with the corresponding word embeddings. Further details are found in Sec. 3.3.3.

3.3. Graph Attention Networks

In this section, we first introduce the general concept of Graph Neural Networks before proceeding to define Visual-GAT and Semantic-GAT.

3.3.1 Graph Neural Networks.

GNNs use the graph structure and node features \mathbf{X}_v to dynamically update the node vector representation [37]. An

anchor node’s features are updated through aggregation—using neighboring features to update the anchor node. If time or multiple layers are involved, then after k aggregation iterations, a given node’s representation encodes updated structural information. The node aggregation operation a_v on node v_i is generically defined as:

$$\begin{aligned} \mathbf{a}_{v_i}^{(k)} &= f_{\text{aggregate}}^{(k)} \left(\left\{ \mathbf{h}_u^{(k-1)} : u \in \mathcal{N}_i \right\} \right) \\ \mathbf{h}_v^{(k)} &= f_{\text{update}}^{(k)} \left(\mathbf{h}_v^{(k-1)}, \mathbf{a}_v^{(k)} \right). \end{aligned} \quad (4)$$

Initially, $\mathbf{h}_{v_i}^{(0)} = \mathbf{X}_v$ and \mathcal{N}_i is the set of nodes adjacent to v_i .

The $f_{\text{aggregate}}^{(k)}(\cdot)$ and $f_{\text{update}}^{(k)}(\cdot)$ functions in GNNs is crucial. Many have been proposed [36]; averaging being a common aggregation method as in Eqtn. 5. We now drop k since our problem consists of a single layer.

$$\begin{aligned} \mathbf{a}_{v_i} &= \frac{1}{|\mathcal{N}_i|} \sum_{j \in \mathcal{N}_i} \mathbf{h}_{v_j} \\ \tilde{\mathbf{h}}_{v_i} &= f_{\text{update}}([\mathbf{h}_{v_i}, \mathbf{a}_{v_i}]) \end{aligned} \quad (5)$$

where, $[\cdot, \cdot]$ is the concatenation operation.

If we consider that in the first step of HOI detection, RPN yield hundreds of proposals, then an averaging method for node features will introduce significant noise. Instead, as proposed in [31], a weighted sum is better suited to mitigate the noise. In this work, we follow the proposal in [31] closely. Consider a virtual node \mathbf{z}_i for a node v_i that is computed as a weighted sum over all neighbors:

$$\mathbf{z}_i = \sum_j \alpha_{ij} \mathbf{h}_{v_j} \quad (6)$$

Weights are given by:

$$\alpha_{ij} = \text{softmax}(f_{\text{attn}}(e_{ij})) \quad (7)$$

where, f_{attn} is a computationally efficient attention function that weighs the importance of node v_j to node v_i and can be implemented through the self-attention neural-net mechanism of [32, 33]. Its parameters are jointly learned with the target task during back propagation without additional supervision.

Once \mathbf{z}_i is computed, then an update mechanism is used to update the output feature $\tilde{\mathbf{h}}_{v_i}$. Specifics about the update will be given for the vision and semantic graphs separately in the subsequent sections.

We now describe custom attention mechanisms in our Visual and Semantic graphs as described in Sec. 3.3.2 and 3.3.3.

3.3.2 Visual Graph Attention Networks

The visual graph instantiates a node v_i from the latent features \mathbf{h}_v of each of detected objects. Then, edge e_{ij} is constructed from the spatial features \mathbf{s}_{ij} from Sec. 3.2. We use an edge function $f_{\text{edge}}(\cdot)$ to integrate the features on the edge along with its two connected nodes according to:

$$\mathbf{h}_{e_{ij}} = f_{\text{edge}}([\mathbf{h}_{v_i}, \mathbf{s}_{ij}, \mathbf{h}_{v_j}]) \quad (8)$$

where, $\mathbf{h}_{e_{ij}}$ are the derived latent features for e_{ij} , with $j \in \mathcal{N}_i$.

We then apply the the attention mechanism of Eqtn. 7 to calculate the distributions of soft weights on each edge and after which we apply a custom weighted sum:

$$\mathbf{z}_{h_i} = \sum_{j \in \mathcal{N}_i} \alpha_{ij} (\mathbf{h}_{v_j} \oplus \mathbf{h}_{e_{ij}}) \quad (9)$$

where, \oplus means element-wise summation operation. Note that latent feature $\mathbf{h}_{e_{ij}}$ includes contextual spatial information.

After that, we leverage a node feature updated function $f_{\text{update}}(\cdot)$ to update each node’s features:

$$\tilde{\mathbf{h}}_{v_i} = f_{\text{update}}([\mathbf{h}_{v_i}, \mathbf{z}_{h_i}]) \quad (10)$$

At this point, we can get an “updated visual graph” with new features as illustrated in Fig. 2. The different edge thickness’ represents the soft weight distributions. In our method, we implement $f_{\text{edge}}(\cdot)$, $f_{\text{attn}}(\cdot)$, and $f_{\text{update}}(\cdot)$ as a single fully-connected layer network with hidden node dimensions of 1024, 1, and 1024 respectively.

3.3.3 Semantic Graph Attention Network

In the semantic graph, word2vec latent representations of the class labels of detected objects are used to instantiate the graph’s nodes. In this graph, we do not assign any features on the edges. We denote \mathbf{w}_i as the word embedding for node i .

As with the visual graph, we use an $f'_{\text{edge}}(\cdot)$ function and an $f'_{\text{attn}}(\cdot)$ function to compute the distributions of soft weights on each edge:

$$\alpha'_{ij} = \text{softmax}(f'_{\text{attn}}(f'_{\text{edge}}([\mathbf{w}_i, \mathbf{w}_j]))). \quad (11)$$

Then, the global semantic features for each node are computed through the linear weighted sum:

$$\mathbf{z}_{w_i} = \sum_{j \in \mathcal{N}_i} \alpha'_{ij} \mathbf{w}_j. \quad (12)$$

After that, we update the node’s features:

$$\tilde{\mathbf{w}}_i = f'_{\text{update}}([\mathbf{w}_i, \mathbf{z}_{w_i}]). \quad (13)$$

As with the visual graph, here too, we output an “updated visual graph” with new features as shown in Fig. 2. Similarly, $f'_{edge}(\cdot)$, $f'_{attn}(\cdot)$, and $f'_{update}(\cdot)$ are designed as single fully-connected layer networks with hidden sizes 1024, 1, and 1024 respectively.

3.4. Combined Graph

To jointly leverage the dynamic information of both the visual and the semantic GATs, it is necessary to fuse them as illustrated in the “Combined Graph” of Fig. 2. The fusion operation can be straightforward however. In this work, we concatenate the features of each of the updated nodes to produce new nodes. We also initialize the edges with the original spatial figures described in Sec. 3.2. We denote the combined node features as γ_i for node i , where $\gamma_i = [\tilde{\mathbf{h}}_{v_i}, \tilde{\mathbf{w}}_i]$.

3.5. Readout and Inference

The last step is to infer the interaction label for a predicate as part of our original triplet <subject, predicate, object>. Note that a person can concurrently perform different actions with each of the available target objects¹. That is, the subject can ‘hold’ or ‘lick’ the knife. In effect, HOI detection is a multi-label classification problem [8]; where, each interaction class is independent and not mutually exclusive.

Thus, to simplify inference, we box-pair specific subject-object bounding boxes ($b_{h_i}, b_{o_{N_i}}$) for all N_i object (nodes) directly linked to the i th human node. [8, 9]. Box-pairing is illustrated in the inference section of Fig. 2.

After box-pairing, we use the final human node representation γ_i , the final object node representation γ_j and mutual spatial edge features s_{ij} to form an action-specific representation $a = [\gamma_i, s_{ij}, \gamma_j]$ for prediction.

First, an action category score $\mathbf{S}_a \in \mathcal{R}^n$ where, n denotes the total number of possible actions, is computed. The computation requires a readout step, whose function $f_{readout}(\cdot)$ is implemented as a multi-layer perceptron² and applied to each action category. The output is then run through a binary sigmoid classifier, which produces the action score as shown in Eqtn. 14.

$$\mathbf{S}_a = \text{sigmoid}(f_{readout}(a)) \quad (14)$$

The final score of a triplet’s predicate \mathbf{S}_R can be computed through the chain multiplication of the action score \mathbf{S}_a , the detected human score s_h from object detection as well as the detected object score s_o as seen in Eqtn. 15:

$$\mathbf{S}_R = s_h * s_o * \mathbf{S}_a. \quad (15)$$

¹ And, it is also possible to have more than one human in an image. We can test only for humans based on their class label

² with 2 hidden layers of dimensions 1024 and 117.

3.5.1 Training

The overall framework is jointly optimized end-to-end, with a multi-class cross-entropy loss that is minimized between action scores and the ground truth action label for each action category:

$$\mathcal{L} = \sum_i \sum_j BCE(\mathbf{S}_{a_{ji}}, Y_{ji}^{label}) \quad (16)$$

We trained our model on 80% HICO-DETs [3] training set, validated on the other 20% and tested with the full range of images in their test set (see Sec. 4.1 for HICO-DETs details).

3.6. Implementation Details

Our architecture was built on Pytorch and the GDL library. For object detection we used Pytorch’s re-implemented Faster-RCNN API [29]. Faster-RCNN used a ResNet-50-FPN backbone [14, 19] trained on the COCO dataset [20]. The object detector and word2vec vectors are frozen during training. We keep the human bounding-boxes whose detection score exceeds 0.8, while for objects we use a 0.3 score threshold.

All neural network layers in our modal are constructed as MLPs as mentioned in previous sections. For training on HICO-DET, we use batch size of 32 and a dropout rate of 0.3. We use an Adam optimizer with a learning rate of 1e-5 and 300 epochs. As for the activation function, we use a LeakyReLU in all attention network layers and a ReLU elsewhere. All experiments are conducted on a single NVIDIA TITAN RTX GPU.

4. Experiments and Results

We evaluate the performance of VS-GATs on the HICO-DET dataset [3] and compare with the SOTA (Table 4.2). Ablation studies are conducted to study the impact of the proposed techniques (Table 4.3). We also visualize the performance distribution of our model across objects for a given interaction (Fig. 3).

4.1. Experimental Setup

Datasets. In this work, we use the HICO-DET data set [3] which builds on top of the HICO dataset [4]. The latter only consists of image-level annotations. HICO-DET on the other hand includes bounding box annotations specifically for the HOI detection task. HICO-DET consists of 38,118 training images and 9,658 testing images. The 117 interaction classes and 80 objects in HICO-DET yield 600 HOI categories in total. The dataset also has 150K annotated human-object pair instances. The dataset is divided into three different HOI categories: (i) Full: all 600 categories; (ii) Rare: 138 HOI categories that have less than 10

Method	Object Detector	Full(600)↑	Rare(138)↑	Non-Rare(462)↑
InteractNet [9]	Faster R-CNN with ResNet-50-FPN	9.94	7.16	10.77
GPNN [28]	Deformable ConvNets [7]	13.11	9.34	14.23
iCAN [8]	Faster R-CNN with ResNet-50-FPN	14.84	10.45	16.15
Xu <i>et al.</i> [36]	Faster R-CNN with ResNet-50-FPN	14.70	13.26	15.13
Gupta <i>et al.</i> [12]	Faster R-CNN with ResNet-152	17.18	12.17	18.68
Li <i>et al.</i> $RP_{T_2}C_D$ [18]	Faster R-CNN with ResNet-50-FPN	17.22	13.51	18.32
PMFNet [34]	Faster R-CNN with ResNet-50-FPN	17.46	15.65	18.00
Peyre <i>et al.</i> [26]	Faster R-CNN with ResNet-50-FPN	19.40	14.60	20.90
Ours(VS-GATs)	Faster R-CNN with ResNet-50-FPN	19.66	15.79	20.81

Table 1. mAP performance comparison with SOTA on the HICO-DET test set.

training instances, and (iii) Non-Rare: 462 HOI categories with more than 10 training instances.

Evaluation Metrics. We use the standard mean average precision (mAP) metric to evaluate the model’s detection performance. mAP is calculated with recall and precision which is common used for the detection task. In this case, we consider a detected result with the form <subject, predicate, object> is positive when the predicted verb is true and both the detected human and object bounding boxes have the intersection-of-union (IoU) exceed 0.5 with respect to the corresponding ground truth.

4.2. Results

4.2.1 Quantitative Results and Comparisons

Our experiments show our model achieves the best mAP results for SOTA in the Full and Rare HOI-DET categories and second best in the Non-Rare category. We achieve gains of +0.26 and +0.14 respectively.

Our multi-cue graph attention mechanism surpasses the performance of works like Peyre *et al.* [26] that exploit functional approximation using visual similarity and thus enabling the system to disambiguate between closely related same-action different-object scenarios. We also outperform works that leveraged human pose like Gupta *et al.* [12] and Wan *et al.* [34]. Pose certainly would be a use-

ful additional cue to incorporate in our work. However, our system still shows better disambiguating ability even without pose cues. We should also note the work of Bansal *et al.* who at this time is yet unpublished but available on pre-prints. They achieve an mAP of 21.96 for the Full category and 16.43 for the Rare category. We did not include this work in our list given that they chose to pre-train their Faster-RCNN implementation directly on the HICO-DET dataset instead of COCO as the rest of the works have done. We think this gives their system an advantage compared to system that train on the more general COCO dataset. By training in this way, the system is able to refine instance proposals and reduce uninformative instances and noise. In our work, we chose not to re-train Faster-RCNN directly on HICO-DET for comparison.

We hold that gains from our works are due to the multi-modal cues leveraged by the dual attention graphs. The graph structure enables the human node to leverage contextual cues from a wide-spread set of (primary and subsidiary) object instances that are dynamically updated by the independent attention mechanisms. Attention learns how—and which—contextual relations aid to disambiguate the inference. This ability is useful for the Rare category which consists of long-tail distribution samples. In conclusion, attending multi-modal cues is a powerful disambiguator. More

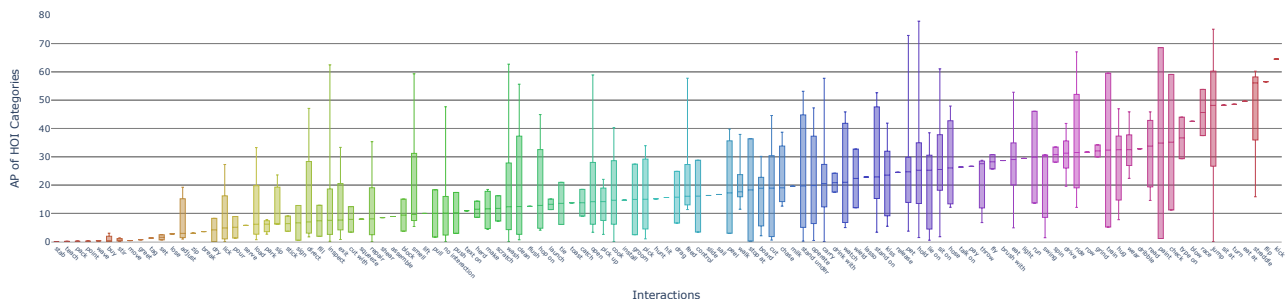


Figure 3. Spread of performance (range and quartiles) across objects for a given interaction. The horizontal axis is sorted by median AP. Plot made with open-source tool provided by [12].

details are presented in Sec. 4.3.

In Fig. 3, we also visualize the performance distribution of our model across objects for a given interaction. As mentioned in [12], it still holds that interactions that occur with just a single object (e.g. 'kick ball' or 'flip skateboard') are easier to detect than those predicates that interact with various objects. Compared to [12], the median AP of interaction 'cut' and 'clean' shown in Fig. 3 outperform those in [12] by a considerable margin because our model does not only use single relation features but subsidiary ones as well.

4.3. Ablation Studies

In our ablation studies we conduct six different tests to understand the performance of each of the different elements of our model. We first describe each test and then analyze the results.

01 Visual Graph Only: G_V only. In this test we remove the Semantic-GAT and keep the Visual-GAT, attention, and inference the same. This study will show the importance of aggregating visual and spatial cues.

02 Semantic Graph Only: G_S only. In this test we remove the Visual-GAT and keep the Semantic-GAT, attention, and inference the same. This study will show the importance of only working with Semantic cues.

03 Without Attention. In this test, we use the averaging attention mechanism of Eqtn. 5 instead of the weighted sum mechanism. We still combine the graphs and infer in the same way.

04 Without Spatial Features in G_C . In this test, we remove spatial features from the edges of the combined graph G_C to study the role that spatial features can play after the aggregation of features across nodes.

05 Message Passing in G_C . In this test, we leverage an additional graph attention network to process the combined graph which is similar to what we do to the original visual-spatial graph. We examine if there would be a gain from an additional message passing step on G_C with combined feature from G_V and G_S .

06 Unified V-S Graph. In this test, we choose to start with a single graph in which visual and semantic features are concatenated in the nodes from the start. Spatial features are still used to instantiate edges. This test examines if there would be a gain from using combined visual-semantic features from the start instead of through separate streams.

We now report on the ablation test results. For the Full category, study 01 yields an mAP of 18.81 which is a large portion of our mAP result suggesting that the visual and spatial features play a primary role in inferring HOI. When only using the Semantic graph in 02, the effect is less marked though still considerable for this single contextual semantic cue. When combining these 3 contextual cues in a graph but not using the attention mechanism

Method	Full \uparrow	Rare \uparrow	Non-Rare \uparrow
Ours(VS-GATs)	19.66	15.79	20.81
01 G_V only	18.81	13.96	20.26
02 G_S only	14.61	11.76	15.46
03 w/o attention	19.01	14.12	20.47
04 w/o spatial features in G_C	18.52	14.28	19.78
05 Message passing in G_C	19.23	14.31	20.70
06 Unified V-S graph	19.39	14.84	20.75

Table 2. mAP performance for various ablation studies.

in test 03, we get a gain bringing the mAP to 19.01. This suggests that edge relations with multi-contextual cues are helpful even without attention. Afterwards, inserting attention but removing spatial features at the end in test 04 hurts. This indicates that spatial features, even after the aggregation stage, are helpful. By inserting spatial features in the combined graph we are basically using a dilated step in neural networks which has also shown to help classification. In test 05, we learn that additional attention in the combined graph does not confer additional benefits. Rather, attention mechanisms for the independent visual-spatial and semantic features are more informative. Similarly with test 06, a combined V-S graph is still not as effective as separating cues early on. Suggesting that visual cues and semantic cues may have some degree of orthogonality to them even though they are related to each other.

5. Conclusion

In this paper we presented a novel HOI detection architecture that studied and leveraged the role of not only primary subject-object contextual cues in interaction, but also the role of subsidiary relations. We showed that multi-modal contextual cues can be graphically represented through Graph Attention Networks to leverage primary and subsidiary contextual relations to disambiguate confusing HOI scenes. Our work ratified this posture by not only exceeding SOTA performance but excelling in classifying Rare categories in HICO-DET.

References

- [1] Ankan Bansal, Sai Saketh Rambhatla, Abhinav Shrivastava, and Rama Chellappa. Detecting Human-Object Interactions via Functional Generalization. *In arXiv preprint arXiv:1904.03181*, 2019. 1, 2
- [2] Joan Bruna, Wojciech Zaremba, Arthur Szlam, and Yann LeCun. Spectral networks and deep locally connected networks on graphs. *In ICLR*, 2014. 2
- [3] Yu-Wei Chao, Yunfan Liu, Xieyang Liu, Huayi Zeng, and Jia Deng. Learning to detect human-object interactions. *In WACV*, pages 381–389. IEEE, 2018. 1, 2, 6
- [4] Yu Wei Chao, Zhan Wang, Yugeng He, Jiaxuan Wang, and Jia Deng. HICO: A benchmark for recognizing human-

- object interactions in images. In *ICCV*, 2015 Inter:1017–1025, 2015. 6
- [5] Rishabh Dabral, Anurag Mundhada, Uday Kusupati, Safer Afaque, Abhishek Sharma, and Arjun Jain. Learning 3D human pose from structure and motion. In *ECCV*, pages 668–683, 2018. 1
- [6] Jifeng Dai, Yi Li, Kaiming He, and Jian Sun. R-FCN: Object detection via region-based fully convolutional networks. In *NIPS*, pages 379–387, 2016. 1
- [7] Jifeng Dai, Haozhi Qi, Yuwen Xiong, Yi Li, Guodong Zhang, Han Hu, and Yichen Wei. Deformable Convolutional Networks. In *ICCV*, pages 764–773, 2017. 7
- [8] Chen Gao, Yuliang Zou, and Jia Bin Huang. ICAN: Instance-centric attention network for human-object interaction detection. In *BMVC*, 2018. 1, 2, 6, 7
- [9] Georgia Gkioxari, Ross Girshick, Piotr Dollár, and Kaiming He. Detecting and Recognizing Human-Object Interactions. In *CVPR*, pages 8359–8367, 2018. 1, 2, 6, 7
- [10] Google. Google Code Archive - Long-term storage for Google Code Project Hosting., 2013. 4
- [11] Marco Gori, Dipartimento Ingegneria, and Gabriele Monfardini. A New Model for Learning in Graph Domains. In *IJCNN*, volume 2, pages 729–734. IEEE, 2005. 2
- [12] Tanmay Gupta, Alexander Schwing, and Derek Hoiem. No-Frills Human-Object Interaction Detection: Factorization, Layout Encodings, and Training Techniques. In *ICCV*, 10 2019. 1, 2, 4, 7, 8
- [13] Kaiming He, Georgia Gkioxari, Piotr Dollár, and Ross Girshick. Mask r-cnn. In *ICCV*, pages 2961–2969, 2017. 1
- [14] Kaiming He, Xiangyu Zhang, Shaoqing Ren, and Jian Sun. Deep residual learning for image recognition. In *CVPR*, pages 770–778, 2016. 4, 6
- [15] Ronghang Hu, Marcus Rohrbach, Jacob Andreas, Trevor Darrell, and Kate Saenko. Modeling relationships in referential expressions with compositional modular networks. In *CVPR*, pages 1115–1124, 2017. 4
- [16] Keizo Kato, Yin Li, and Abhinav Gupta. Compositional learning for human object interaction. In *ECCV*, pages 234–251, 2018. 2
- [17] Maosen Li, Siheng Chen, Xu Chen, Ya Zhang, Yanfeng Wang, and Qi Tian. Actional-Structural Graph Convolutional Networks for Skeleton-based Action Recognition. In *Arxiv 1904.12659*, 2019. 1, 2
- [18] Yong-Lu Li, Siyuan Zhou, Xijie Huang, Liang Xu, Ze Ma, Hao-Shu Fang, Yan-Feng Wang, and Cewu Lu. Transferable Interactiveness Knowledge for Human-Object Interaction Detection. In *CVPR*, 2018. 1, 4, 7
- [19] Tsung Yi Lin, Piotr Dollár, Ross Girshick, Kaiming He, Bharath Hariharan, and Serge Belongie. Feature pyramid networks for object detection. In *CVPR*, pages 936–944, 2017. 4, 6
- [20] Tsung Yi Lin, Michael Maire, Serge Belongie, James Hays, Pietro Perona, Deva Ramanan, Piotr Dollár, and C. Lawrence Zitnick. Microsoft COCO: Common objects in context. In *ECCV*, pages 740–755, 2014. 6
- [21] Wei Liu, Dragomir Anguelov, Dumitru Erhan, Christian Szegedy, Scott Reed, Cheng Yang Fu, and Alexander C. Berg. SSD: Single shot multibox detector. In *ECCV*, pages 21–37. Springer, 2016. 1
- [22] Cewu Lu, Ranjay Krishna, Michael Bernstein, and Li Fei-Fei. Visual relationship detection with language priors. In *ECCV*, pages 852–869. Springer, 2016. 2
- [23] Tomas Mikolov, Ilya Sutskever, Kai Chen, Greg S Corrado, and Jeff Dean. Distributed representations of words and phrases and their compositionality. In *NIPS*, pages 3111–3119, 2013. 2, 4
- [24] Mathias Niepert, Mohamed Ahmed, and Konstantin Kutikov. Learning convolutional neural networks for graphs. In *ICML*, pages 2014–2023, 2016. 2
- [25] Dario Pavllo, Christoph Feichtenhofer, David Grangier, and Michael Auli. 3D human pose estimation in video with temporal convolutions and semi-supervised training. In *Proceedings of the IEEE Conference on Computer Vision and Pattern Recognition*, pages 7753–7762, 2019. 1
- [26] Julia Peyre, Ivan Laptev, Cordelia Schmid, and Josef Sivic. Detecting unseen visual relations using analogies. In *ICCV*, pages 1981–1990, 2019. 1, 2, 7
- [27] Bryan A Plummer, Arun Mallya, Christopher M Cervantes, Julia Hockenmaier, and Svetlana Lazebnik. Phrase localization and visual relationship detection with comprehensive image-language cues. In *ICCV*, pages 1928–1937, 2017. 4
- [28] Siyuan Qi, Wenguan Wang, Baoxiong Jia, Jianbing Shen, and Song Chun Zhu. Learning human-object interactions by graph parsing neural networks. In *ECCV*, pages 407–423, 2018. 3, 7
- [29] Shaoqing Ren, Kaiming He, Ross Girshick, and Jian Sun. Faster R-CNN: Towards Real-Time Object Detection with Region Proposal Networks. In *NIPS*, pages 91–99, 2015. 1, 4, 6
- [30] Franco Scarselli, Marco Gori, Ah Chung Tsoi, Markus Hagenbuchner, and Gabriele Monfardini. Computational capabilities of graph neural networks. *IEEE Transactions on Neural Networks*, 20(1):81–102, 2008. 2
- [31] Chen Sun, Abhinav Shrivastava, Carl Vondrick, Rahul Sukthankar, Kevin Murphy, and Cordelia Schmid. Relational Action Forecasting. In *CVPR*, pages 273–283, 2019. 3, 5
- [32] Ashish Vaswani, Noam Shazeer, Niki Parmar, Jakob Uszkoreit, Llion Jones, Aidan N. Gomez, Łukasz Kaiser, and Illia Polosukhin. Attention is all you need. In *NIPS*, pages 5999–6009, 2017. 5
- [33] Petar Veličković, Arantxa Casanova, Pietro Liò, Guillem Cucurull, Adriana Romero, and Yoshua Bengio. Graph attention networks. In *ICLR*, 2018. 3, 5
- [34] Bo Wan, Desen Zhou, Yongfei Liu, Rongjie Li, and Xuming He. Pose-aware Multi-level Feature Network for Human Object Interaction Detection. In *ICCV*, pages 9469–9478, 2019. 1, 2, 7
- [35] Zonghan Wu, Shirui Pan, Fengwen Chen, Guodong Long, Chengqi Zhang, and Philip S. Yu. A Comprehensive Survey on Graph Neural Networks. *Arxiv 1901.00596*, pages 1–22, 2019. 2

- [36] Bingjie Xu, Yongkang Wong, Junnan Li, Qi Zhao, and Mohan S Kankanhalli. Learning to Detect Human-Object Interactions with Knowledge. In *In CVPR*, pages 2019–2028, 2019. 1, 3, 5, 7
- [37] Keyulu Xu, Stefanie Jegelka, Weihua Hu, and Jure Leskovec. How powerful are graph neural networks? In *In ICLR*, 2019. 4
- [38] Sijie Yan, Yuanjun Xiong, and Dahua Lin. Spatial temporal graph convolutional networks for skeleton-based action recognition. In *AAAI*, pages 7444–7452, 2018. 1
- [39] Jianwei Yang, Jiasen Lu, Stefan Lee, Dhruv Batra, and Devi Parikh. Graph R-CNN for Scene Graph Generation. In *In ECCV*, pages 690–706, 2018. 3, 4
- [40] Hanwang Zhang, Zawlin Kyaw, Shih-Fu Chang, and Tat-Seng Chua. Visual translation embedding network for visual relation detection. In *In CVPR*, pages 5532–5540, 2017. 4
- [41] Bohan Zhuang, Lingqiao Liu, Chunhua Shen, and Ian Reid. Towards Context-Aware Interaction Recognition for Visual Relationship Detection. In *In ICCV*, pages 589–598, 10 2017. 4